Research Article | Vol. 10, No. 5 | 1 May 2019 | BIOMEDICAL OPTICS EXPRESS 2275
Biomedical Optics EXPRESS

Development of a flow cell based Raman spectroscopy technique to overcome photodegradation in human blood

Ben Hansson,[1,5] Christian Harry Allen,[1,5] Sami Qutob,[2] Bradford Behr,[3] Balazs Nyiri,[4] Vinita Chauhan,[2] and Sangeeta Murugkar [1,*]

[1]*Department of Physics, Carleton University, 1125 Colonel By Drive, Ottawa, ON K1S 5B6, Canada*
[2]*Consumer and Clinical Radiation Protection Bureau, Healthy Environments and Consumer Safety Branch, Health Canada, K1A 0K9, Ottawa, Canada*
[3]*Tornado Spectral Systems, 555 Richmond Street West, Suite 402, Toronto, ON M5V 3B1, Canada*
[4]*Department of Medical Physics, The Ottawa Hospital Cancer Centre, Ottawa, ON K1H 8L6, Canada*
[5]*Equal contribution*
**smurugkar@physics.carleton.ca*

Abstract: Raman spectroscopy of blood offers significant potential for label-free diagnostics of disease. However, current techniques are limited by the use of low laser power to avoid photodegradation of blood; this translates to a low signal to noise ratio in the Raman spectra. We developed a novel flow cell based Raman spectroscopy technique that provides reproducible Raman spectra with a high signal to noise ratio and low data acquisition time while ensuring a short dwell time in the laser spot to avoid photodamage in blood lysates. We show that our novel setup is capable of detecting minute changes in blood lysate spectral features from natural aging. Moreover, we demonstrate that by rigorously controlling the experimental conditions, the aging effect due to natural oxidation does not confound the Raman spectral measurements and that blood treated with hydrogen peroxide to induce oxidative stress can be discriminated from normal blood with a high accuracy of greater than 90% demonstrating potential for use in a clinical setting.

1. Introduction

Raman spectroscopy (RS) is a well-established vibrational spectroscopy technique for performing non-destructive, label-free, real-time characterization of chemical mixtures. It involves the inelastic scattering of laser light due to vibrations of molecular bonds and provides a "chemical fingerprint" of the specimen [1]. RS has been demonstrated to be a powerful biomedical diagnostic technique and has been widely applied to detect distinct disease-related abnormalities in cells and tissue [2]. The analysis of biofluids such as blood, urine and saliva [3] using RS is a rapidly emerging area of research. This is because biofluids present a rich source of information related to multiple disease biomarkers and hence offer the potential to be a powerful diagnostic and prognostic tool correlating with patient health. Moreover, such samples are readily accessible in a minimally invasive manner compared to organ tissue biopsies. In particular, RS of blood and its constituents has been investigated as a promising approach in a variety of applications ranging from assessing the health status of patients [4,5] to applications in forensics [6].

Blood is composed of ~50% plasma that mostly contains water, 40-45% red blood cells (RBCs) that mostly contain hemoglobin, and relatively small proportion of white blood cells (WBCs)/platelets. Although there have been significant efforts in developing *in vivo* applications involving the detection of glucose and other analytes [7,8] in whole blood, the majority of applications of RS to detect disease markers in blood have focused on developing *in vitro* assays to investigate the status of RBCs, WBCs or blood plasma and serum, which is obtained by removing the dissolved protein fibrinogen and clotting factors from the plasma.

#357247 https://doi.org/10.1364/BOE.10.002275
Journal © 2019 Received 14 Jan 2019; revised 14 Mar 2019; accepted 15 Mar 2019; published 4 Apr 2019

Biomedical Optics EXPRESS

For example, proof-of-principle studies have successfully demonstrated that RS of blood plasma/serum can discriminate between healthy controls and oral cancer [9], head and neck cancer [10], and prostate cancer [11] with sensitivity and specificity above 75%. RS has also been applied to investigate intact RBCs and hemoglobin to detect biomarkers related to malaria, diabetes, genetic blood disorders, and heart failure [5]. These studies demonstrate the significant potential of *in vitro* RS of blood for disease diagnostics.

The optical instrumentation and techniques employed for *in vitro* Raman blood analysis have been mainly based on laser tweezers Raman spectroscopy [12,13], surface enhanced Raman scattering (SERS) spectroscopy [14,15] and dried drop RS [3,16]. However, there can be potential challenges associated with these techniques such as: requirement for isolating the RBCs and long data acquisition times involved, in the case of laser tweezers-based optical trapping [5]; the lack of reproducibility of the Raman signal in SERS-based detection [17]; and sample inhomogeneity in the dried drop methods [18]. In addition, a critical requirement common to these techniques is to avoid laser induced photodegradation of the blood caused by the strongly absorbing hemoglobin, which also gives rise to a broad fluorescence background in the Raman spectra. Longer laser wavelength in the near-infrared is generally preferred in order to minimize the fluorescence from hemoglobin, but this typically results in weaker Raman signal strength owing to its inverse relationship with the fourth power of the laser excitation wavelength [5]. The weak Raman signal can be amplified by increasing the laser power, but this increases the risk of photodegradation in the blood. In fact, even at relatively low laser power levels of 5 mW (power density of ~2.5 $MWcm^{-2}$) and an acquisition time of ~100 s, the 785 nm laser beam focused on single trapped RBCs can cause irreversible photodamage of hemoglobin [19]. This damage threshold of hemoglobin is even lower at ~0.1 $MWcm^{-2}$ at a lower laser excitation wavelength at 632.8 nm [20] and at ~0.01 $MWcm^{-2}$ in the case of a dried blood drop sample [21]. However, at such low laser power densities, RS is not ideal and does not give an adequate spectrum with a good signal to noise ratio in a short data acquisition time using current techniques.

The present study thus aims to overcome these limitations related to the RS of blood. We demonstrate for the first time a novel flow cell based RS technique to provide reproducible Raman spectral measurements of blood lysate at 785 nm. The use of lysed blood (blood lysate) instead of individual RBCs is advantageous since it simplifies sample preparation and accessibility: there is no additional preparation step of RBC isolation and blood samples can be conveniently frozen at −80 °C until use. Moreover, it simplifies the Raman spectroscopy setup as it does not involve optical trapping of cells. We show that flowed blood measurements are advantageous over static blood measurements that are representative of current techniques and that the short dwell time of 0.4 s in the laser spot with a power density of less than 0.2 $MWcm^2$ avoids photodamage and still provides a high signal to noise ratio. The other advantages of the setup constructed from off-the-shelf optical components include i) ease of sample manipulation using a reusable quartz flow cell ii) optimized excitation and collection of the Raman scattered light using a water immersion objective iii) homogenous sampling of the blood lysate volume due to an adjustable flow rate and iv) access to a large data set of Raman spectra for a given blood lysate sample, without manual sample placement and alignment. We show that our novel setup is capable of detecting minute changes in blood lysate spectral features from natural aging. Moreover, we demonstrate that by rigorously controlling the experimental conditions, the aging effect does not confound the Raman spectral measurements and that blood treated with hydrogen peroxide to induce oxidative stress, can be discriminated from normal blood with an accuracy of greater than 90%.

Biomedical Optics EXPRESS

2. Materials and methods

2.1 Samples

Peripheral blood was drawn with informed consent from healthy volunteers following procedures approved by Health Canada's Research Ethics Committee (REB-2002-012). Blood was drawn via periphery venipuncture into 2 x 10 ml EDTA vacutainer tubes (Becton Dickinson and Company, Franklin Lakes, NJ). 3 ml of blood taken from one donor was aliquoted into 5 ml flow tubes (BD Biosciences, San Jose, CA, USA). The blood was rocked at room temperature for three hours and then immediately frozen at −80 °C to induce hemolysis. Frozen blood samples were thawed overnight in a 4 °C fridge. Thawed blood lysate samples were mixed gently and drawn inside a 1 mL syringe for measurements with the flow cell based RS setup as described in Section 2.2. This procedure was repeated three times using the same donor. The measurements were acquired using blood lysate that was flowing as described in Section 2.2 or in static form. In this case, the blood lysate was pumped into the flow cell and then held static in the flow cell for measurement with the syringe pump turned off. The blood lysate sample will be simply referred to as 'blood' in the rest of the article except when noted otherwise.

Oxidative stress was induced in fresh blood by treatment with hydrogen peroxide, a source of reactive oxygen species [22]. Fresh blood samples were aliquoted into 3 ml and placed into flow tubes. Hydrogen peroxide at the appropriate concentration was added drop-by-drop to the blood. Samples comprised two controls (no peroxide) and two dosed samples that were prepared at 20 mM and 100 mM using a 30% hydrogen peroxide stock solution (Sigma-Aldrich, Canada, Oakville, ON, Canada). Following treatment with hydrogen peroxide, the samples were kept on a rocker for three hours and then immediately frozen at −80°C until Raman acquisitions.

2.2 Construction of the flow cell-based Raman spectroscopy setup

Figure 1 shows a schematic of the custom-built Raman spectroscopy and flow cell setup. Raman excitation is provided by a variable power, multi-mode 785 nm diode laser (Ondax, Monrovia, CA, U.S.A.) with a maximum power of 500 mW coupled into a 100 µm core, 0.22 NA multimode fiber. A lens of focal length 40 mm (lens L1 in Fig. 1) collimates the multimode fiber-coupled output such that it slightly overfills the back aperture of a 60X, 1.1 NA water immersion microscope objective (Olympus Canada Inc., Richmond Hill, ON, Canada). A 785 nm band pass filter (Iridian, Ottawa, ON, Canada) is inserted in the incident laser beam path to remove the fluorescence generated in the fiber. The use of a water immersion objective instead of an air objective to focus the laser on the blood lysate sample enables better matching of the refractive indices across the blood/quartz and water interface and thus results in higher Raman signal collection [23]. The multimode laser beam is focused to a spot whose lateral diameter and depth of focus was measured to be 12 µm and 25 µm respectively [24]. The lateral diameter of the laser spot was empirically determined from a calibrated bright field image of the focused laser spot while the depth of focus was determined by acquiring Raman spectra from various heights at the surface of a polystyrene dish [25]. The laser power density can be varied from 0 - 165 $kWcm^{-2}$ at the sample focal plane corresponding to 0 - 200 mW of average power. Raman scattered light from the sample is collected by the objective and passed through a 785 nm long pass dichroic mirror (Iridian) and two long pass edge filters (Iridian) to completely remove the laser excitation. This is coupled to a 300 µm core multimode fiber (Thorlabs, Newton, NJ, U.S.A.) which delivers the Raman signal to a Tornado HyperFlux U1 spectrometer (Tornado Spectral Systems, Toronto, ON, Canada). The setup also includes a bright-field imaging capability utilizing a white LED source and CCD camera (Thorlabs) in the back-reflection configuration; this subsystem is useful for setting an appropriate flow rate inside the flow-cell as described below in Section 2.3.1.

Biomedical Optics EXPRESS

The Raman flow cell consists of a quartz capillary tube and two syringe pumps. The thin-walled (0.01 mm) capillary tube is composed of boron-rich quartz and has an internal diameter of 1.5 mm (Charles Supper Company, Natick, MA, U.S.A.). This is embedded within a lengthwise channel milled atop a solid (25 mm x 50 mm) aluminum slide and held in place from either end using duct tape. The slide is secured on an aluminum round block of diameter 55 mm and height 15 mm for mounting on an automated xyz stage (Applied Scientific Instrumentation Inc., Eugene, OR, U.S.A.). A well of diameter 5 mm and depth 1 mm in the round aluminum block traps a drop of water over the quartz capillary tube, allowing the water immersion objective to be used.

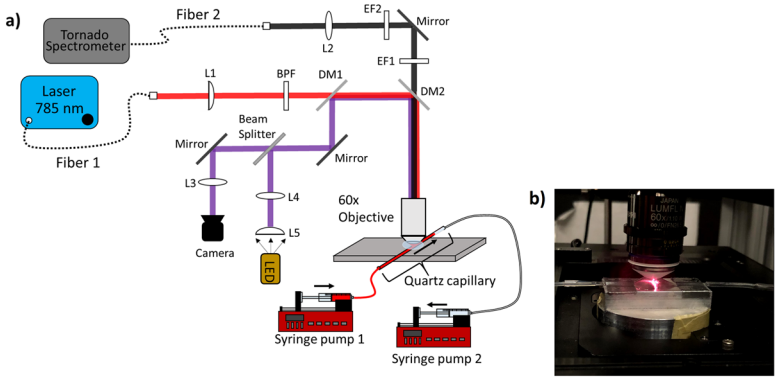

Fig. 1. (a) Schematic of the Raman spectroscopy probe consisting of Lenses L1 – L5; BPF: 785 nm bandpass filter; EF1 and EF2: > 800 nm edge filters to transmit the Raman light only, DM1 and DM2 are dichroic mirrors (b) Close-up photograph of the water-immersion objective to excite and collect the laser and Raman-scattered light respectively from the blood sample in the flow cell.

Flow through the capillary was achieved using two syringe pumps (New Era Pump Systems, Farmingdale, NY, U.S.A.) and two 1 mL syringes (BD, Franklin Lakes, NJ, U.S.A.). The pumps were paired such that the pump with sample provided positive pressure and the second (empty) pump provided negative pressure, achieving steady flow of the sample through the system. At the end of measurements, pump direction was reversed such that all sample returned to the first syringe. The system could be reused by flushing any remaining sample out first with 100% sodium hypochlorite (bleach), followed by three times flushing with distilled water.

2.3. System characterization methods

Initial characterization of the flow-cell based RS setup was performed to establish optimal parameters related to the sampling depth inside the flow cell, the flow rate, laser power density and exposure time. The objective was to minimize the laser exposure time without sacrificing Raman signal strength.

2.3.1. Flow cell characterization

Flow properties of the system were characterized by axial velocity measurements of 5 µm polystyrene beads (Phosphorex Inc., MA, U.S.A.) in water flowing through the system. A series of bright field images of the flowing beads at a given depth inside the tube were analyzed in ImageJ, to determine the flow velocity at that depth. This method was repeated at different depths inside the tube.

2.3.2. Measurement of the Raman signal for flowed and static blood

The characterization of the Raman signal was done on static (syringe pump off) and flowed blood (syringe pump on) with the objective of determining the performance of the flowed blood

Biomedical Optics EXPRESS

measurements compared to static blood measurements that represent current techniques. For the comparison between static and flowed blood, 14 static time series (STS) and 14 flow time series (FTS) were collected for three different samples of blood from the same donor. Each time series was composed of 100 consecutive 2s Raman spectra. The laser was initially shuttered and the blood was static. Then the blood was flowed with a dwell time of 0.4 s, or 30 μm/s at the focal depth, for a 30 s duration to reach a steady-state flow condition. The laser was un-shuttered and a 200 s time series of the flowed blood was acquired. After the FTS, the laser was shuttered and the flow continued for 30 s to obtain a fresh sample of blood. The flow was stopped and the system was allowed to settle to a static state (zero flow) over 60 s. Then the laser was un-shuttered again and a single volume of blood was exposed to the laser for 200 s corresponding to a single STS. Finally, the laser was re-shuttered and the same method repeated until a total of 14 STS and 14 FTS were acquired.

For the dependence of the Raman signal on laser power, the laser power was set to maximum of 187 mW at the sample and the power density at the sample was varied using neutral density filters. 5 STS and 5 FTS were each gathered for a low (20 $kWcm^{-2}$), medium (83 $kWcm^{-2}$), and high (165 $kWcm^{-2}$) laser power density corresponding to average power of 23, 94 and 187 mW respectively at the sample.

2.4. Raman spectral measurements of normal and hydrogen peroxide treated blood

This study was performed on blood flowing in the quartz tube at a flow rate of 2.2 uL/min with a dwell time of 0.22 s of the laser exposure and a power density of 120 kW cm^{-2}. The total measurement time T_m, for one blood sample, including the time for loading the blood sample into the flow cell, the time for acquiring 500 Raman spectra of flowed blood, followed by the time for cleaning of the flow cell, was carefully monitored. A protocol was developed so that each control or peroxide treated blood sample was exposed to ambient oxygen for the same amount of time T_m. This ensured that each blood sample had been oxidized/aged by the same amount. The typical T_m was 50 minutes and measurements were performed in triplicate for each dose group.

2.5. Spectral processing and statistical analysis

The Raman spectra were background corrected using a baseline subtraction algorithm known as SNIP [26] and normalized using vector normalization. The SNIP technique determines a baseline to subtract from the spectrum by finding the minimum between a given point and the average value of the outer edges of a window centered on that point. This is done iteratively with the window size reducing by one on either side until it reaches a size of 1, at which point it stops. An initial window width of 111 indices was used for this experiment.

Welch's t-test was used to evaluate Raman spectral differences between the initial 20 s (first 10 spectra) and the final 20 s of data acquisition over 14 time series of 200 s each, for static and flowed blood. The Wilcoxon rank sum test was used to test for statistically significant differences ($p < 0.05$) between the median ratio of specific Raman band intensities for blood treated with 20 mM and 100 mM concentration of hydrogen peroxide relative to the median ratio for the control blood.

Principal component analysis (PCA) and Linear Discriminant Analysis (LDA) was performed in Mathematica (Wolfram Research, IL, U.S.A.) using standard algorithms. PCA is an unsupervised classification tool used to reduce the dimensionality of the data while preserving most of the variations (both what is sought for and the random noise). It produces a new set of orthogonal variables, called principal components (PCs). PCA-LDA is a technique that uses PCA for dimensional reduction of the spectroscopic data set and LDA for the supervised classification of this prepared data set. LDA finds the direction in PC space along which the difference between the two classes is maximal relative to the random variations.

Biomedical Optics EXPRESS

3. Results and discussion

3.1 System characterization results

The experiments and data analysis were aimed at determining the optimal experimental conditions for the Raman spectra of blood.

3.1.1 Characterization of the flow cell

The Raman spectra for static blood were obtained as a function of the depth inside the flow cell as shown in Fig. 2(a). At a depth of 0 µm at the surface of the quartz tube, the Raman spectrum is dominated by the Raman signal from quartz. The intensity of the Raman signal from 100 - 600 µm deep inside the flow cell has ~5% attenuation per 100 µm as seen in Fig. 2(a). Thus, a depth of 100 µm gives the maximum Raman signal while minimizing the quartz background. Based on these data, the depth of measurement for the Raman spectra of blood was fixed at 100 µm for the rest of this study.

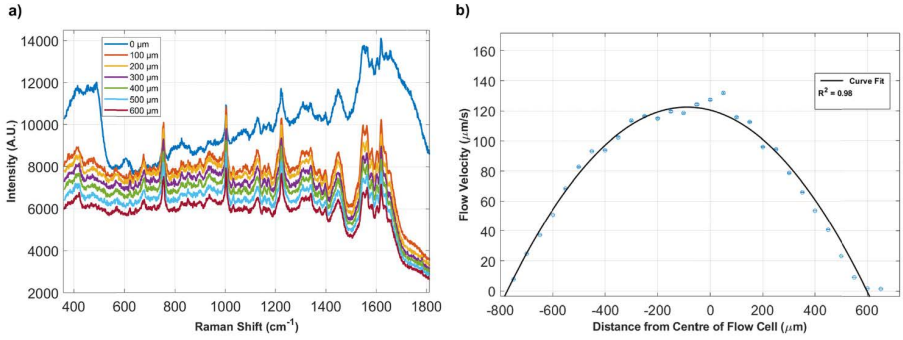

Fig. 2. (a) Raman spectra of blood at varying depths inside the flow cell. (b) Parabolic velocity distribution of 5 µm polystyrene beads in water flowing through the quartz capillary tube, obtained by increasing the depth of the laser focal spot into the tube.

The velocity of a fluid flowing in a tube of diameter d as a function of distance r from the center of the tube is described by the following equation [27]

$$v(r) = v_0\left(1-\left(\frac{2r}{d}\right)^2\right) \tag{1}$$

where the velocity at the center of the tube is v_0. The flow rate Q can be expressed as

$$Q = \frac{1}{8}\pi d^2 v_0 \tag{2}$$

In our measurements, the laser is focused at a depth d_{focal} of 100 µm below the surface of the quartz tube of diameter d = 1.5 mm (radius R = 0.75 mm). For the dwell time t_{dwell}, the time that a given volume of blood would be exposed to the focused laser spot of 12 µm diameter at this depth, the velocity $v(r)$ is

$$v(r) = v_0\left(1-\left(\frac{2\left(R-d_{focal}\right)}{d}\right)^2\right) = 12\,\mu\text{m}/t_{dwell} \tag{3}$$

To standardize a flow rate, the requirement was set such that a given volume of blood would be exposed to the focused laser spot for t_{dwell} = 0.4 s. This meant that for a Raman data acquisition time of 2 s, the Raman signal would be sampled from at least 5 different blood volumes flowing at a velocity of 30 µm/s. From Eqs. (1) and (2), the flow rate was estimated

Biomedical Optics EXPRESS

to be Q = 5.5 µL/min and the flow rate on the syringe pump was set to this value for all the results reported here. Results of the measurements of the velocity of 5 µm polystyrene beads in water flowing through the quartz capillary tube as described in Section 2.3.1, are plotted in Fig. 2(b). A parabolic distribution of axial velocity vs. depth in the tube, that is characteristic of laminar flow, is evident in Fig. 2(b). Furthermore, the Reynolds number for the flowing blood was calculated to be 0.024 for the flow rate used. This places the blood in the very low Reynolds number regime [28,29] and fulfills the R < 2400 requirement for laminar flow.

3.1.2. Raman spectra of blood at varying laser power densities

Raman spectra were obtained from flowed and static blood at three different laser power densities. As shown in the representative data in Fig. 6 in the appendix, the Raman spectra are dominated by the vibrational modes of hemoglobin as expected. The tentative molecular band assignments are given in Table 1 in the appendix and are consistent with previous reports of Raman spectra of whole blood and RBCs [15,30]. It is important to note that the Raman spectra do not show any evidence of new peaks at 975, 1248, 1366 and 1396 cm^{-1} even at the highest power density (165 $kWcm^{-2}$) employed. These peaks appear if there is photodegradation associated with protein denaturation or hemoglobin aggregation [19,20,30,31]. The absence of these Raman peaks in our measurements suggests that the blood samples are not being photodamaged at the laser powers and exposures times employed.

3.2. Detection of aging effects in the Raman spectra of blood

The flow cell based RS setup is highly sensitive in detecting changes in blood as it ages due to auto-oxidation. Figure 3 shows a comparison of the mean of the Raman spectra of the first and last time series separated by 160 minutes for the static blood and flowed blood. The fluorescence background decreases as a function of time for both static and flowed blood in Fig. 3(a) and Fig. 3(b). The mean of the background-subtracted Raman spectra for the first and last time series for static and flowed blood, are shown in Fig. 3(c) and 3(d) respectively. The difference spectra between the first and last time series for static blood and flowed blood are shown in Fig. 3(e) and 3(f). Similar changes are evident in the intensities of Raman peaks for the static and flowed blood. This is expected since the blood aging process will affect both static and flowed blood. In particular, there is a significant increase in the intensity of the Raman peaks at 570, 1224, 1375, 1398, 1582 and 1635 cm^{-1} and a decrease in the intensities corresponding to the 788, 1211, 1545 and 1604 cm^{-1} Raman peaks in the mean spectrum corresponding to the last time series. These Raman bands are highlighted in Fig. 3(c) – 3 (f).

The Raman peak at 570 cm^{-1} is associated with the FeO_2 stretching of the central iron atom of the globin unit and the peak at 1635 cm^{-1} corresponds to the asymmetric C-C stretching mode of the porphyrin skeleton in the hemoglobin molecule. Both of these peaks are known to be sensitive to the oxygenation status of the hemoglobin molecule and increase in intensity upon oxygenation [32,33]. The peaks at 1211 and 1224 cm^{-1}, correspond to the methane deformation mode and are sensitive to the changes in the deformation angle of the methane group that are caused by conformational changes in the hemoglobin. A decrease in the intensity of the 1211 cm^{-1} Raman peak with a concomitant increase in the intensity of the 1224 cm^{-1} peak correlates with the increase in the oxygenation state of the hemoglobin molecules [20,30,32,33]. The vibration modes at 1341, 1375 and 1390 cm^{-1} associated with the pyrrole half ring stretch are considered to be the oxidation state markers of the central iron atom within the porphyrin macrocycle. The increase in the intensity of the peaks at 1375 and 1390 cm^{-1} as seen in the mean spectrum of the last time series indicates the conversion from the ferrous (Fe^{+2}) to the more oxidized ferric (Fe^{+3}) state.

Biomedical Optics EXPRESS

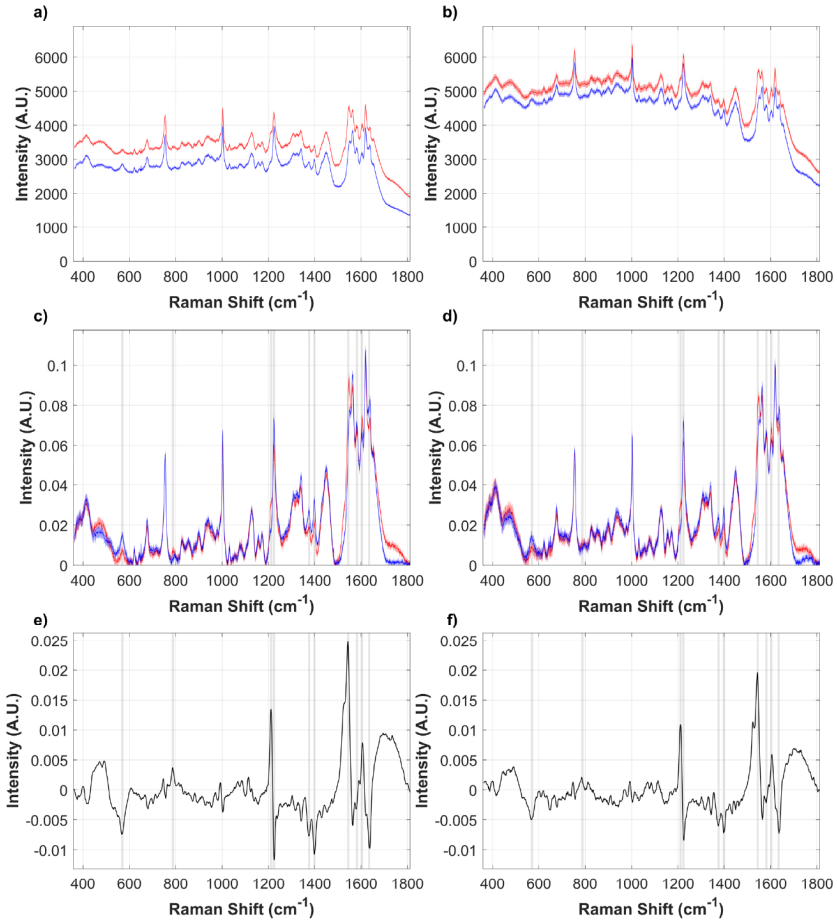

Fig. 3. Comparison of the Raman spectra from the first and the last time series separated by 160 minutes. Mean intensity along with a 95% confidence interval of the Raman spectra in the first (red) and last (blue) time series for (a) static blood and (b) flowed blood. Background-subtracted Raman spectra for the first and last time series separated by 160 minutes for (c) static blood and (d) flowed blood. Difference spectrum between the first and last time series for (e) static blood and (f) flowed blood.

The Raman peaks at 1546, 1563, 1582, 1603, 1620 and 1635 cm^{-1} correspond to the in-plane vibration modes of the porphyrin and correlate with the spin state of the iron atom. A decrease in the intensity of the Raman peaks at 1546 and 1604 cm^{-1} with an accompanying increase in the intensity of the 1582 and 1635 cm^{-1} Raman peaks signifies a transition of Fe from a high spin state to a low spin state, which is a characteristic of oxygenated hemoglobin [30–32]. This is consistent with earlier reports related to the Raman spectra of aged blood [15,21,34]. Therefore, our experiments reveal changes in the Raman spectra that are consistent with the natural aging of blood due to auto-oxidation.

3.3. Comparison of the Raman spectra of flowed and static blood

Figures 4(a) and 4(b) show the mean intensity along with a 95% confidence interval of the first 10 (red), middle 10 (blue) and last 10 (green) Raman spectra in the first STS (a) and FTS (b) over 200 s for one data set. It is evident that the background fluorescence decreases with time in the static blood but not in the flowed blood. This is consistent with the well-known photobleaching effect in blood [35]. We next set out to determine whether there was a

Biomedical Optics EXPRESS

significant difference in the Raman spectral peak intensities as a function of time, for a single time series corresponding to static and flowed blood. The mean intensity and standard deviation of the Raman spectra after background subtraction corresponding to the first 10 (red) and last 10 (blue) spectra of 14 time series for one data set are plotted for static blood (c) and for flowed blood (d) respectively. Welch's t-test was performed to determine if the group (n = 14) of the mean intensity of the Raman peaks in the first 10 spectra of all 14 time series was significantly different from that of the last 10 spectra of all 14 time series, for static and flowed data sets.

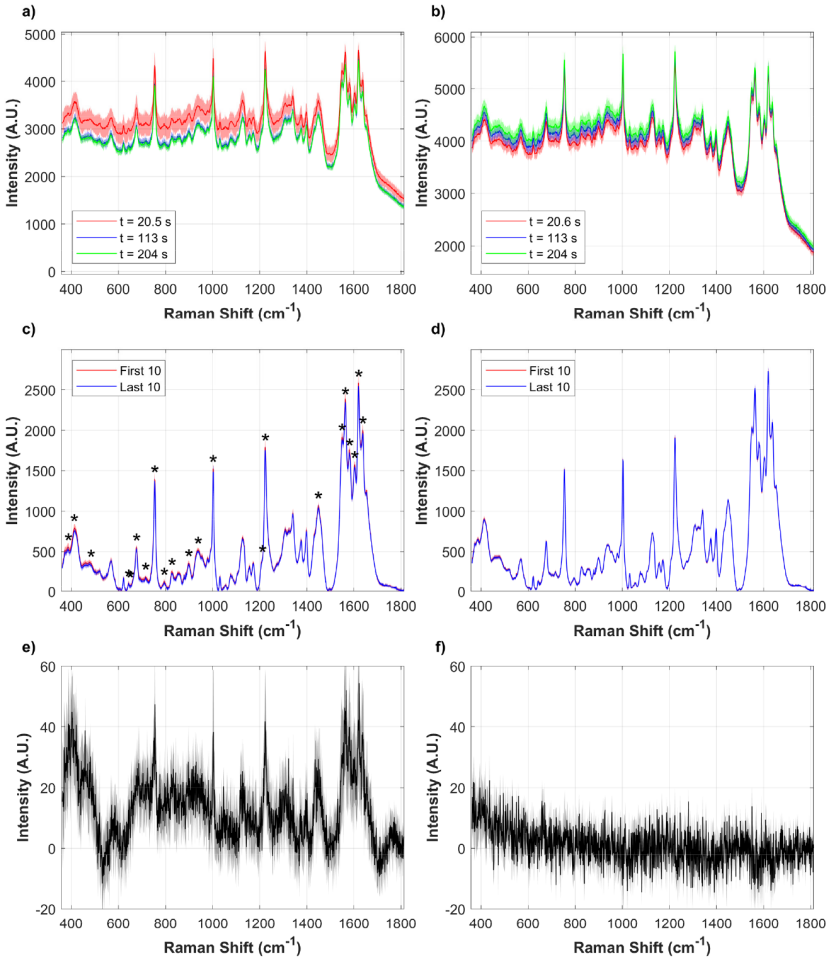

Fig. 4. Plot of the mean intensity and along with a 95% confidence interval of the first 10 (red), middle 10 (blue) and last 10 (green) Raman spectra in the first time series for (a) static blood and (b) flowed blood. (c) and (d) Background-corrected Raman spectra showing the mean intensity and standard deviation of the first 10 (red) and last 10 (blue) spectra of all 14 time series for (c) static blood and (d) flowed blood. The mean of (n = 14 time series) difference spectra between the mean of the first 10 spectra and the last 10 spectra for each time series, along with 95% confidence interval, for static (e) and flowed blood (f).

It is evident that there are significant differences in the Raman spectra ($p < 0.05$) as a function of time for static blood; these are indicated by a * in the plots. In contrast, there are no differences in the Raman spectra over 200 s in the flowed blood (Fig. 4(d)). This is also seen in Fig. 4(e) and 4(f) which displays the mean of (n = 14 time series) difference spectra between the mean of the first 10 spectra and the last 10 spectra for each time series, along with 95% confidence interval, for static and flowed blood respectively. The longer laser exposure time of

Biomedical Optics EXPRESS

200 s for the static blood volume could be causing photoinduced oxidation in the static blood as shown in previous reports [21,36–38]. In contrast each flowed blood volume is exposed to the focused laser spot for only 0.4 s at the 100 µm depth inside the quartz flow cell. This exposure time is too short to cause any noticeable changes in the Raman spectra. Hence the flowed blood yields more reproducible results.

3.4. Discrimination between normal and hydrogen peroxide treated blood

The flow cell based RS technique was tested to determine if biochemical differences between blood treated with different doses of hydrogen peroxide could be detected despite the effects of auto-oxidation of blood. Flowed blood measurements were performed under strictly controlled conditions as described in Section 2.4. Figure 5(a) shows the mean of the Raman spectra along with the 95% confidence interval for the mean for the data from three separate sets of Raman spectral measurements for each of the control blood (n = 4455 spectra) and dosed blood samples (n = 1485 spectra for 20 mM and n = 1485 spectra for 100 mM concentration of hydrogen peroxide). It should be noted that the blood samples are from a single donor and measurements were made over 3 days using 3 technical replicates.

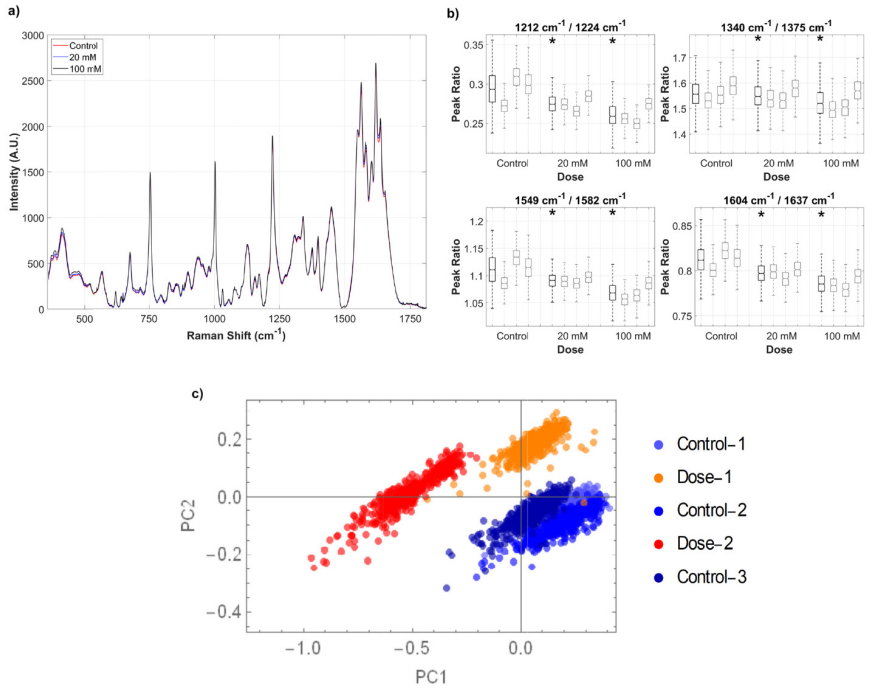

Fig. 5. (a) Mean of the Raman spectra along with the 95% confidence interval corresponding to control blood (n = 4455) and blood treated with 20 mM (n = 1485) and 100 mM concentration (n = 1485) of hydrogen peroxide. (b) Tukey style box plots showing the variation in the ratio of the intensity of Raman bands at: 1212 cm^{-1} and 1224 cm^{-1}; 1340 cm^{-1} and 1375 cm^{-1}; 1549 and 1582 cm^{-1}; and 1604 cm^{-1} and 1637 cm^{-1} for each dose group. Black boxes consist of all spectra for a given dose, while grey boxes are all spectra for a given day for a given dose. Outliers have been left out for clarity and * indicates statistically significant differences ($p < 0.05$) between the median ratios for the dosed group relative to the control group using all spectra. (c) PCA scatter plot for a Raman data set of three control samples (Control-1,2,3) and the two dosed samples (Dose-1 and Dose-2 correspond to 20 mM and 100mM concentration of hydrogen peroxide). The order of the plot legend reflects the order of consecutive measurements.

There are very small differences noticeable in Fig. 5(a) at 1212, 1224, 1375, 1549, 1604 and 1637 cm^{-1} which are known to be Raman biomarkers for oxidation [38]. Figure 5(b) is a

Biomedical Optics EXPRESS

compilation of Tukey style box plots using this data to show the variation in the ratio of the intensity of Raman bands at: 1212 cm^{-1} and 1224 cm^{-1}; 1340 cm^{-1} and 1375 cm^{-1}; 1549 and 1582 cm^{-1}; and 1604 cm^{-1} and 1637 cm^{-1}. The Wilcoxon rank sum test revealed that there is a statistically significant shift ($p < 0.05$) towards decreasing values for the median ratio (black boxes in Fig. 5(b)) of the blood treated with 20 mM and 100 mM concentration of hydrogen peroxide relative to the median ratio for the control blood in each of the four subplots. This tendency of the decreasing intensity ratio of the marker Raman bands corresponds to the increasing oxygenation of the blood associated with the higher concentrations of hydrogen peroxide treatment and is consistent with earlier reports [36–38].

PCA was performed on each data set consisting of three control samples and the two dosed samples (n = 480 per sample, after removing the top and bottom 2% of the total intensity distribution). A scatter plot of the scores for the first two PCs of one Raman data set (Fig. 5(c)) shows excellent clustering of individual Raman spectra as a function of the hydrogen peroxide dose. PCA-LDA of this data set produced a classification accuracy of close to 99.8%. After combining three different data sets, the classification accuracy was lowered to ~90%. This type of batch effect has been observed earlier [39]. Even better control of sample preparation and processing conditions should reduce this batch effect.

4. Conclusion

The RS technique involving a custom-built flow cell setup demonstrated in this work, provides reproducible results from flowed blood lysates with a high signal to noise ratio and without photodamage. Current RS techniques that measure Raman spectra from static blood samples in the form of a drop or from RBCs, are not only susceptible to photodamage, but are extremely labour-intensive [5,21]. This is because they involve considerable sample manipulation for obtaining a large data set that is an unbiased representation of the sample population. In contrast, our technique does not require additional sample preparation steps of isolating RBCs and does not involve long integration times. The automated and reusable flow cell design of our RS technique enables homogenous sampling and makes the collection of a large data set of Raman spectra from different blood samples easily feasible. The optimized excitation and collection of the Raman scattered light using a water immersion objective lens provides sensitive detection of pathological changes in the Raman spectra of blood. In fact, we demonstrate that our technique is capable of detecting very small differences due to the aging effect in blood (e.g. oxygenation state). Moreover, we show that by rigorously controlling the experimental conditions for sample testing, our technique is able to overcome external interfering factors such as aging, and detect small differences in blood exposed to oxidative stress induced by hydrogen peroxide. By using a smaller (micro) capillary tube as a sample holder, our method could be readily applied to smaller (≤100 μL) volumes of blood or other sample fluids that are more difficult to obtain clinically. The optical setup could be further compacted for portability, enabling clinical translation and further support of retrospective biodosimetry. In this latter case the use of frozen lysed blood offers the practicality of sample preservation where immediate analysis is not possible. The same technique could readily be applied to investigate other individual blood components such as RBCs, WBCs, plasma and serum.

Biomedical Optics EXPRESS

Appendix

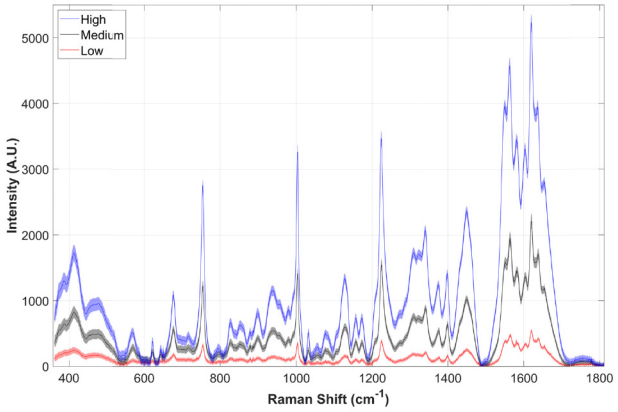

Fig. 6. Raman spectra of flowed blood at high (165 kWcm^{-2}), medium (83 kWcm^{-2}), and low (20 kWcm^{-2}) laser power densities.

Table 1. Tentative molecular assignments for the main peaks observed in the Raman spectra of lysed human blood [12,15,29]. Abbreviations: (ν) & (δ) in-plane modes, (γ) out-of-plane modes, (str) stretch, (p) protein, (Phe) and phenylalanine.

Raman Shift (cm^{-1})	Assignment
413	δ (Fe-O-O)
518	protein: S-S stretching
568	ν (Fe-O_2)
622	Phenylalanine: C–C twist
644	protein: C-S stretching
677	ν_7
716	γ_{11}
754	ν_{15}
787	ν_6
826	γ_{10}
855	γ_{10}
899	protein: C-C skeletal
935	ν_{46}
979	protein: skeletal vibration **or** deoxyribose
1002	phenylalanine
1032	δ (CH_2)
1077	δ (= $C_bH_2)_{asym}$ asymmetric stretching
1127	ν_5
1157	ν_{44}
1172	ν_{30}
1211	$\nu_5 + \nu_{18}$
1223	ν_{13} **or** ν_{42}
1307	ν_{21}
1341	ν_{41}
1376	ν_4
1399	ν_{20}
1450	δ (CH_2 - CH_3)
1549	ν_{11}
1563	ν_{19}
1582	ν_{37}
1604	hemoglobin: ν (C = C)
1619	hemoglobin: ν (C = C)
1638	ν_{10}
1654	Amide I

Biomedical Optics EXPRESS

Funding

The Natural Sciences and Engineering Research Council of Canada (NSERC)-Discovery Grant (SM - RGPIN-2015-06154); NSERC-Engage Grant (SM and BB - EGP 521982-17).

Acknowledgments

We greatly appreciate the support of Philippe Gravel at Carleton University in machining the custom mount for the flow cell, Mike Antunes at Carleton University for providing neutral density filters, and Iridian Spectral Technologies, Ottawa for the optical filters used in the Raman spectroscopy setup. We thank Nadine Adam at Health Canada for her help in preparing the blood samples.

Disclosures

The authors declare that there are no conflicts of interest related to this article.

References

1. H. J. Butler, L. Ashton, B. Bird, G. Cinque, K. Curtis, J. Dorney, K. Esmonde-White, N. J. Fullwood, B. Gardner, P. L. Martin-Hirsch, M. J. Walsh, M. R. McAinsh, N. Stone, and F. L. Martin, "Using Raman spectroscopy to characterize biological materials," Nat. Protoc. **11**(4), 664–687 (2016).
2. K. Kong, C. Kendall, N. Stone, and I. Notingher, "Raman spectroscopy for medical diagnostics--From in-vitro biofluid assays to in-vivo cancer detection," Adv. Drug Deliv. Rev. **89**, 121–134 (2015).
3. M. J. Baker, S. R. Hussain, L. Lovergne, V. Untereiner, C. Hughes, R. A. Lukaszewski, G. Thiéfin, and G. D. Sockalingum, "Developing and understanding biofluid vibrational spectroscopy: a critical review," Chem. Soc. Rev. **45**(7), 1803–1818 (2016).
4. A. J. Berger, T. W. W. Koo, I. Itzkan, G. Horowitz, and M. S. Feld, "Multicomponent blood analysis by near-infrared Raman spectroscopy," Appl. Opt. **38**(13), 2916–2926 (1999).
5. C. G. Atkins, K. Buckley, M. W. Blades, and R. F. B. Turner, "Raman Spectroscopy of Blood and Blood Components," Appl. Spectrosc. **71**(5), 767–793 (2017).
6. K. Virkler and I. K. Lednev, "Raman spectroscopic signature of blood and its potential application to forensic body fluid identification," Anal. Bioanal. Chem. **396**(1), 525–534 (2010).
7. A. M. K. Enejder, T. W. Koo, J. Oh, M. Hunter, S. Sasic, M. S. Feld, and G. L. Horowitz, "Blood Analysis by Raman Spectroscopy," Opt. Lett. **27**(22), 2004–2006 (2002).
8. J. Chaiken, J. Goodisman, B. Deng, R. J. Bussjager, and G. Shaheen, "Simultaneous, noninvasive observation of elastic scattering, fluorescence and inelastic scattering as a monitor of blood flow and hematocrit in human fingertip capillary beds," J. Biomed. Opt. **14**(5), 050505 (2009).
9. A. Sahu, S. Sawant, H. Mamgain, and C. M. Krishna, "Raman spectroscopy of serum: an exploratory study for detection of oral cancers," Analyst (Lond.) **138**(14), 4161–4174 (2013).
10. A. T. Harris, A. Lungari, C. J. Needham, S. L. Smith, M. A. Lones, S. E. Fisher, X. B. Yang, N. Cooper, J. Kirkham, D. A. Smith, D. P. Martin-Hirsch, and A. S. High, "Potential for Raman spectroscopy to provide cancer screening using a peripheral blood sample," Head Neck Oncol. **1**(1), 34 (2009).
11. D. K. R. Medipally, A. Maguire, J. Bryant, J. Armstrong, M. Dunne, M. Finn, F. M. Lyng, and A. D. Meade, "Development of a high throughput (HT) Raman spectroscopy method for rapid screening of liquid blood plasma from prostate cancer patients," Analyst (Lond.) **142**(8), 1216–1226 (2017).
12. A. Bankapur, E. Zachariah, S. Chidangil, M. Valiathan, and D. Mathur, "Raman Tweezers Spectroscopy of Live, Single Red and White Blood Cells," PLoS One **5**(4), e10427 (2010).
13. J. Lin, L. Shao, S. Qiu, X. Huang, M. Liu, Z. Zheng, D. Lin, Y. Xu, Z. Li, Y. Lin, R. Chen, and S. Feng, "Application of a near-infrared laser tweezers Raman spectroscopy system for label-free analysis and differentiation of diabetic red blood cells," Biomed. Opt. Express **9**(3), 984–993 (2018).
14. X. Zhang, N. C. Shah, and R. P. Van Duyne, "Sensitive and Selective Chem/ Bio Sensing Based on Surface-Enhanced Raman Spectroscopy (SERS)," Vib. Spectrosc. **42**(1), 2–8 (2006).
15. W. R. Premasiri, J. C. Lee, and L. D. Ziegler, "Surface-Enhanced Raman Scattering of Whole Human Blood, Blood Plasma, and Red Blood Cells: Cellular Processes and Bioanalytical Sensing," J. Phys. Chem. B **116**(31), 9376–9386 (2012).
16. K. W. C. Poon, F. M. Lyng, P. Knief, O. Howe, A. D. Meade, J. F. Curtin, H. J. Byrne, and J. Vaughan, "Quantitative reagent-Free Detection of Fibrinogen Levels in Human Blood Plasma using Raman Spectroscopy," Analyst (Lond.) **137**(8), 1807–1814 (2012).
17. A. Bonifacio, S. Dalla Marta, R. Spizzo, S. Cervo, A. Steffan, A. Colombatti, and V. Sergo, "Surface-enhanced Raman spectroscopy of blood plasma and serum using Ag and Au nanoparticles: a systematic study," Anal. Bioanal. Chem. **406**(9-10), 2355–2365 (2014).
18. F. Bonnier, F. Petitjean, M. J. Baker, and H. J. Byrne, "Improved protocols for vibrational spectroscopic analysis of body fluids," J. Biophotonics **7**(3-4), 167–179 (2014).

Biomedical Optics EXPRESS

19. R. Dasgupta, S. Ahlawat, R. S. Verma, A. Uppal, and P. K. Gupta, "Hemoglobin degradation in human erythrocytes with long-duration near-infrared laser exposure in Raman optical tweezers," J. Biomed. Opt. **15**(5), 055009 (2010).
20. B. R. Wood, L. Hammer, L. Davis, and D. McNaughton, "Raman microspectroscopy and imaging provides insights into heme aggregation and denaturation within human erythrocytes," J. Biomed. Opt. **10**(1), 014005 (2005).
21. P. Lemler, W. R. Premasiri, A. DelMonaco, and L. D. Ziegler, "NIR Raman spectra of whole human blood: Effects of laser-induced and in vitro hemoglobin denaturation," Anal. Bioanal. Chem. **406**(1), 193–200 (2014).
22. E. Zachariah, A. Bankapur, C. Santhosh, M. Valiathan, and D. Mathur, "Probing oxidative stress in single erythrocytes with Raman Tweezers," J. Photochem. Photobiol. B **100**(3), 113–116 (2010).
23. L. M. Fullwood, G. Clemens, D. Griffiths, K. Ashton, T. P. Dawson, R. W. Lea, C. Davis, F. Bonnier, H. J. Byrne, and M. J. Baker, "Investigating the use of Raman and immersion Raman spectroscopy for spectral histopathology of metastatic brain cancer and primary sites of origin," Anal. Methods **6**(12), 3948–3961 (2014).
24. C. H. Allen, "Raman Spectroscopy of Human Lens Epithelial Cells Exposed to a Low-dose Range of Ionizing Radiation," MSc Thesis, Carleton University, Ottawa (2018).
25. P. Caspers, G. Lucassen, H. Bruining, and G. Puppels, "Automated depth scanning confocal Raman microspectrometer for rapid in vivo determination of water concentration profiles in human skin," J. Raman Spectrosc. **31**(8-9), 813–818 (2000).
26. M. Morhác and V. Matousek, "Peak Clipping Algorithms for Background Estimation in Spectroscopic Data," Appl. Spectrosc. **62**(1), 91–106 (2008).
27. P. Nelson, *Biological Physics. Energy, Information, Life* (Freeman and Company, 2014), Chap. 5.
28. K. Avila, D. Moxey, A. de Lozar, M. Avila, D. Barkley, and B. Hof, "The Onset of Turbulence in Pipe Flow," Science **333**(6039), 192–196 (2011).
29. M. Kersaudy-Kerhoas, R. Dhariwal, M. P. Y. Desmulliez, and L. Jouvet, "Hydrodynamic blood plasma separation into microfluidic channels," Microfluid. Nanofluidics **8**(1), 105–114 (2010).
30. B. R. Wood, P. Caspers, G. J. Puppels, S. Pandiancherri, and D. McNaughton, "Resonance Raman Spectroscopy of Red Blood Cells Using Near-Infrared Laser Excitation," Anal. Bioanal. Chem. **387**(5), 1691–1703 (2007).
31. M. A. S. de Oliveira, Z. J. Smith, F. Knorr, R. E. de Araujo, and S. Wachsmann-Hogiu, "Long term Raman spectral study of power-dependent photodamage in red blood cells," Appl. Phys. Lett. **104**(10), 103702 (2014).
32. S. Barkur, D. Mathur, and S. Chidangil, "A laser Raman tweezers study of eryptosis," J. Raman Spectrosc. **49**(7), 1155–1164 (2018).
33. B. R. Wood, B. Tait, and D. McNaughton, "Micro-Raman characterisation of the R to T state transition of haemoglobin within a single living erythrocyte," Biochim. Biophys. Acta **1539**(1-2), 58–70 (2001).
34. K. Buckley, C. G. Atkins, D. Chen, H. G. Schulze, D. V. Devine, M. W. Blades, and R. F. B. Turner, "Non-invasive spectroscopy of transfusable red blood cells stored inside sealed plastic blood-bags," Analyst (Lond.) **141**(5), 1678–1685 (2016).
35. B. Deng, C. Wright, E. Lewis-Clark, G. Shaheen, R. Geier, and J. Chaiken, "Direct noninvasive observation of near infrared photobleaching of autofluorescence in human volar side fingertips in vivo," Proc. SPIE **7560**, 75600 (2010).
36. R. Liu, L. Zheng, D. L. Matthews, N. Satake, and J. W. Chan, "Power dependent oxygenation state transition of red blood cells in a single beam optical trap," Appl. Phys. Lett. **99**(4), 043702 (2011).
37. S. Ahlawat, N. Kumar, R. Dasgupta, R. S. Verma, A. Uppal, and P. K. Gupta, "Raman spectroscopic investigations on optical trap induced deoxygenation of red blood cells," Appl. Phys. Lett. **103**(18), 183704 (2013).
38. S. Ahlawat, N. Kumar, A. Uppal, and P. Kumar Gupta, "Visible Raman excitation laser induced power and exposure dependent effects in red blood cells," J. Biophotonics **10**(3), 415–422 (2017).
39. H. Moradi, A. Ahmad, D. Shepherdson, N. H. Vuong, G. Niedbala, L. Eapen, B. Vanderhyden, B. Nyiri, and S. Murugkar, "Raman micro-spectroscopy applied to treatment resistant and sensitive human ovarian cancer cells," J. Biophotonics **10**, 1327–1334 (2016).